CrystEngComm

The Relationship between the Crystal Habit and the Energy Framework Pattern: A Case Study Involving Halogen Bonding on the Edge of a Covalent Bond

Journal:	*CrystEngComm*
Manuscript ID	CE-ART-04-2023-000316.R1
Article Type:	Paper
Date Submitted by the Author:	01-May-2023
Complete List of Authors:	Torubaev, Yury; Ben-Gurion University of the Negev; Weizmann Institute of Science Howe, Devin; Ball State University Leitus, Gregory; Weizmann Institute of Science, Chemical Research Support Unit Rosokha, Sergiy; Ball State University, Chemistry

The Relationship between the Crystal Habit and the Energy Framework Pattern: A Case Study Involving Halogen Bonding on the Edge of a Covalent Bond

Yury V. Torubaev,[a,b]* Devin Howe,[c] Gregory Leitus,[d] and Sergiy V. Rosokha[c]*

[a] *Department of Chemistry, Ben-Gurion University of the Negev, Beer-Sheva 84105, Israel.*
[b]*Department of Molecular Chemistry and Materials Science, Weizmann Institute of Science, Rehovot 7610001, Israel.*
[c] *Department of Chemistry, Ball State University. Muncie, IN 47306, USA*
[d]*Department of Chemical Research Support, Weizmann Institute of Science, Rehovot 7610001, Israel*

Abstract

The relationship between solid-state supramolecular interactions and crystal habits is highlighted based on experimental and computational analysis of the crystal structure of strong halogen-bonded (HaB) associations between iodine-containing dihalogens (ICl, IBr) with 1,4-diazabicyclo[2,2,2]octane (DABCO) as well as with substituted pyridines and phenazine. The pattern of the energy frameworks and the interplay of the attractive and repulsive interactions in the solid-state associations involving these HaB donors and acceptors directly correlated with their crystal habits. This correlation suggests that analysis of the energy framework serves as a useful tool (complementary to the earlier developed methods) to rationalize and predict the crystal habit. The X-ray structural analysis also revealed that the I···N distances in the complexes were in the 2.24 Å – 2.54 Å range, i.e. they were much closer to the I···N covalent bond length than to the van der Waals separation. The computational analysis of the nature of halogen bonding in these complexes showed delocalization of their molecular orbitals' between donor and acceptors resulting in a substantial charge transfer from the nucleophiles to dihalogens and elongation of the I···X bond. As a result, both I···N and I···X bonds in the strongest complexes (e.g., ICl with DABCO or 4-dimethylaminopyridine) are characterized by the comparable Mayer bonds orders of about 0.6, along with the electron and energy densities at their bond critical points of about 0.1 a.u. and -0.02 a.u., respectively. These data as well as the density overlap regions indicator (DORI) point to the covalency of the I···N bonding and suggest that the interaction within the IX complexes can be described as (unsymmetrical) hypervalent 3c/4e N···I···X bonding akin to that in trihalide or halonium ions.

Keywords: halogen bonding, co-crystals, energy framework, crystal habit, crystal morphology.

Introduction.

Since the pioneering work in crystallography, the question of how the external shape of the crystals reflects their internal structures has remained one of the essential topics of interest within the chemical community.[1-3] The factors governing the crystal habit and morphology can be divided into two subcategories: internal (e.g., crystal symmetry, unit cell geometry, intermolecular interaction) and external (e.g., solvent, additives, kinetics of crystals growth). Elucidation of the external factors allows clarifying the mechanism of the crystal growth, inducing the formation of the desired polymorph and/or achieving a certain amount of control over the crystal habit and phase composition. These tasks are important in many applications, and, therefore, the effect of the solvents and additives was extensively studied by Doherty, Leiserowitz, Aquilano, and other researchers.[4-8] The relationship between the internal structure and exterior of an ideal crystal is most frequently interpreted using the Hartman and Perdok periodic bond chain (PBC) theory.[9,10] This method (and its later revisions [11-13]) states that the fastest growth occurs in the direction of the face that is crossed by the largest number of chains of strong interactions. Crystal morphology prediction tool based on the Bravais, Friedel, Donnay, and Harker (BFDH) approximation (utilizing crystallographic geometric and symmetry considerations) is included in Mercury, a commonly used software for the analysis and visualization of X-ray structural data.[14-17]

The growing interest in halogen bonding and other σ- and π-hole supramolecular interactions inspired the extensive research of the co-crystals.[18-24] Besides the numerous applications in pharmacology, material science, etc., co-crystallization has been used to tune the crystal habit.[23-26] For example, co-crystallization of sulfonamides with 4,4′-dipyridyl produced block-like crystals, which were better suited for the single-crystal X-ray diffraction studies than the needle-like crystals of the original substance.[27] In our recent studies of the co-crystallization of diphenyl ditelluride or organometallic halides with the σ- and π–hole donors, we noted the relationship between the columnar or layered topology of the energy frameworks and the needle or the plate-like habits of the respective crystals.[28,29] In order to corroborate these relationships in the molecular co-crystals, we examined in the current work the associations of the

iodo-dihalogens ICl, IBr, and I_2 with aliphatic and aromatic nucleophiles, in particular, 1,4-diazobicyclo[2,2,2]octane, pyridine, 2-bromopyridine, 4-dimethylaminopyridine and phenazine (abbreviated hereinafter as DABCO, Py, PyBr, $PyNMe_2$ and Phnz, respectively).

The diatomic iodo-containing molecules are among the strongest neutral halogen bond (HaB) donors. The adduct of I_2 with ammonia was the first system that is nowadays considered halogen-bonded (HaB) complex.[19,30,31] The interaction of dihalogens with various nucleophiles has been fruitfully utilized in various areas from crystal engineering and the capture of radioactive iodine to organocatalysis.[31-34] Earlier studies showed that I_2 formed very strong 1:1 and 2:1 associations with DABCO in solution, which were referred to as charge-transfer complexes.[35,36] More recent X-ray structural analyses revealed that co-crystallization of DABCO and I_2 produced 1:1 and 1:2 complexes in the solid state as well.[37] The N···I distance of 2.37 Å, reported for the 1:1 complex, was much closer to the N-I covalent bond length than to the van der Waals separation of these atoms.[37] Analogous short I…N distances were observed in the 2:1 complexes of ICl with fullerene-fused DABCO and in the 1:1 complex of IBr with cationic (N-methylsubstituted) DABCO.[38, 39] We showed earlier that adjusting the strength of HaB donor in the complexes of bromosubstituted electrophiles with DABCO or variation of HaB acceptor in the complexes of I_2 with aromatic N-oxides allows one to gradually modulate the strength (and ultimately, the nature) of interactions in such associations from supramolecular to covalent bonding.[40, 41] Wide variations of N···I distances were also observed in complexes of I_2, IBr, and ICl molecules with pyridine derivatives.[42] In fact, the N···I bond of 2.246 Å in the complex of ICl with 4-dimethylaminopyridine[43] is even shorter than that in the association of DABCO with I_2. Such strong N···I interactions raise the question if the amine – interhalogen associates should be considered in crystallization modeling as two-component systems or as single molecular units, and they suggest the detailed study of the nature of bonding in these systems. Thus, the goals of this work are to evaluate the relationship between the crystal habit and the energy framework pattern in a series of complexes of IX molecules with aliphatic and aromatic amines and to examine the nature and properties of N···I halogen bonding on the edge of a covalent bond.

2. Results and discussion.

2.1. X-ray structural characterization of DABCO·IX complexes

Mixing hexane solutions of DABCO with the respective interhalogen (ICl or IBr) in a 1:1 molar ratio resulted in the instant precipitation of a yellow to orange microcrystalline product. These substances were recrystallized from hot acetonitrile (see the Experimental part for details) to afford rhombic (isomorphic) plates suitable for single-crystal X-ray structural studies. Their X-ray analysis revealed isostructural 1:1 complexes DABCO·ICl and DABCO·IBr, which are shown in Figure 1.

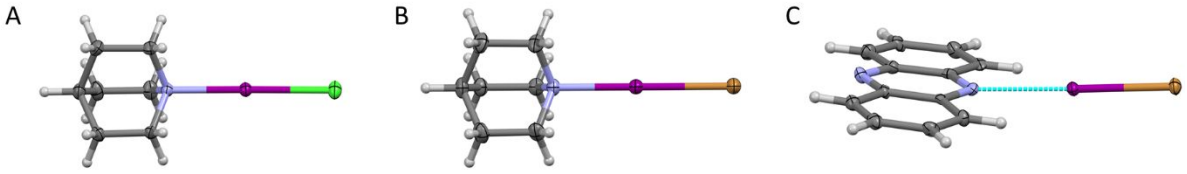

Figure 1. X-ray structures of DABCO·ICl (A), DABCO·IBr (B), and Phnz·IBr (C) (see the crystal lattices in Figure S1 in the Supporting Information).

Evaporation of a solution containing equimolar quantities of IBr and phenazine produced pale-yellow needles. X-ray analysis showed that these crystals comprised 1:1 complexes Phnz·IBr, which are also illustrated in Figure 1. Selected geometric characteristics of these complexes are listed in Table 1.

Table 1. Selected characteristics of the solid-state (amine)·IX complexes.

Complex	$d_{N\cdots I}$, Å	$d_{I\cdots X}$, Å	$\angle_{N\cdots I\cdots X}$, deg	E,[a] kJ/mol
DABCO·ICl	2.274	2.604	179.4	-96
DABCO·IBr	2.303	2.702	179.8	-81
DABCO·I_2[b]	2.366	2.854	178.4	-62
$PyNMe_2$·ICl[c]	2.246	2.562	179.2	-78
Py·ICl[d]	2.284	2.523	179.2	-61
PyBr·ICl[e]	2.350	2.476	177.8	-34
Phnz·IBr	2.541	2.576	178.8	-33

a) Intermolecular interaction energy between N and I atoms in the solid-state complexes of IX determined using CrystalExplorer [52]. b) Ref.37. c) Ref. 43. d) Ref. 44. e) Ref. 45.

In addition, this table includes the characteristics of the HaB complexes of ICl with pyridine derivatives $PyNMe_2$·ICl,[43] Py·ICl, and PyBr·ICl,[45] and 1:1 complex of DABCO with I_2[37] whose structures had

been previously reported without an emphasis on their morphology or the energy of intermolecular interactions. In all these systems, the associations with ICl and IBr showed an almost linear N···I-X (X = Br, Cl) fragment (type-II halogen-halogen interaction).[11,46] The I···N separations in complexes with the same HaB acceptor decreased in the order: I_2 > IBr > ICl. The decrease of the I···N separations was accompanied by the increase of interaction energies between these atoms (calculated using CrystalExplorer [52], see the Experimental section for details). These variations in the HaB length and strength in the amine·IX complexes (Table 1) are generally consistent with the changes in the maximum electrostatic potential on the surfaces of the HaB donors ($V_{s\,max}$) and the most negative potentials $V_{s\,min}$ on the N atom of amine (which are illustrated in Figure S2 in the Supporting Information). Analogous bond length variations were previously observed in complexes of dihalogens with hexamethylenetetramine and pyridines [53] and in the step-wise HaB of 1,4-diiodotetrafluorobenzene with multidentate polypyridines.[54]

Most notably, the HaB lengths in all these amine·IX complexes were 32-39% shorter than the sum of the van der Waals radii of nitrogen and iodine (1.55 Å and 2.17 Å, respectively [47,48]). Accordingly, they were only 10-20% longer than the covalent N-I bond (~ 2.05 Å [49,50]). The I-X bond lengths in the complexes were 5 - 12 %, longer as compared to the individual molecules (2.321 Å, 2.469 Å, and 2.665 Å in ICl, IBr, and I_2, respectively).[51] Overall, the energetic and geometry characteristics of N···I interactions suggest that the co-crystals in Table 1 they can be considered, at least for the purpose of crystal structure modeling, as essentially single component systems. To clarify the nature of these interactions, the analysis of the crystal habits (section 2.2) is followed by the computational study of the N···I bonding (section 2.3).

2.2. Energy framework pattern and crystal habit of the co-crystals.

Pronounced platelet and acicular habits of crystals of ICl or IBr with DABCO, pyridines and phenazine prompted investigation into the potential relationship between their supramolecular structures and crystal habits. In particular, co-crystals of DABCO with ICl and IBr are characterized by nearly ideal rhombic plate-like shapes illustrated in Figure 2A. The analysis of the intermolecular contacts in these crystals revealed a distinct layered pattern (Figure 2B and Figure S3 in the Supporting Information).

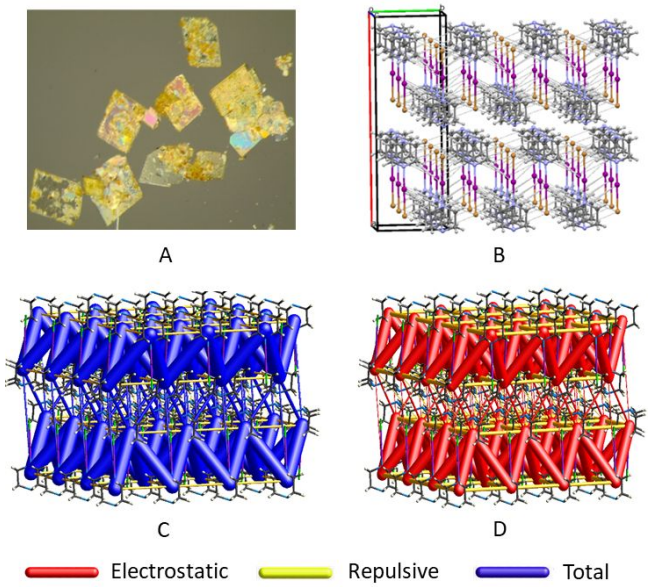

Figure 2. (A) Plate-like crystals of DABCO·IBr. (B) The crystal lattice of DABCO·IBr showing the layers of the HaB complexes. Hydrogen bonds are shown as light gray lines. (C, D) Energy frameworks of DABCO·IBr showing the chains of strong intermolecular interactions propagating predominantly along the layers of the HaB complexes (color code: blue – the total intermolecular interaction energy; yellow – repulsive, predominantly electrostatic, interactions; red – electrostatic contribution to the total energy, note that the dispersion contributions are shown in Figures S3 and S4 in the Supporting Information).

The combination of the layered crystal structure and its platelet habit is consistent with the PBC theory,[9, 10, 55] since the crystal faces (100) in DABCO·ICl and DABCO·IBr, which cross more *chains of strong* H···X (X = Cl, Br) *interactions,* are expected to grow faster. However, the distances between layers of molecules, between centers of mass in molecules and even between two atoms of two adjacent molecules are not as reliable measures of the strength of bonding as the distance between covalently bonded atoms. Therefore, consideration of the strength of intermolecular bonding based on the short/long distance criteria might be misguiding.[56] Furthermore, multiple short contacts in acicular crystals of interhalogens with pyridines or phenazine either does not allow to detach certain dominant packing pattern in their structures, or assemble their molecules into the H---Cl hydrogen bonded (HB) layers, which appear orthogonal to the longest dimension of the needles.

The combination of BFDH approximation with the force field computations allows, in some cases, reliable prediction of crystal morphology.[11] Yet, it is computationally expensive and does not visualize

the correlation between the molecular packing pattern and crystal morphology. It is also noteworthy, that based on the shortest intermolecular distances and *Pbcn* symmetry, the (BFDH-based) Mercury software [14] correctly suggests the rhombic shape of DABCO·IB crystals. However, the predicted axes do not agree with their indexed directions [010] and [001] (Figure S5 in the Supporting Information).

The Crystal Explorer's, which combines efficient calculation of intermolecular interaction energies with a graphical representation of their magnitude, is a perfect tool to visualize and analyze the chains of strong interactions.[52,57] In the co-crystals of DABCO with ICl or IBr**,** they propagate in two dimensions in (100) plane. As a result, (100) is the main crystal face (Figure 2C, D). The energy frameworks of co-crystals of interhalogens with pyridines and phenazine showed the 1D chains of uninterrupted strong interactions resulting in their acicular habit (Figure 3 and Figure S6 in the Supporting Information). The directions of these chains perfectly match the longest direction of the crystal. (Note that Crystal Explorer plots energy frameworks as the cylinders connecting the centers of the mass of molecules, i.e. zig-zag lines. The respective chain of strong interaction can be considered as a straight line, see Figure S7 in the Supporting Information).

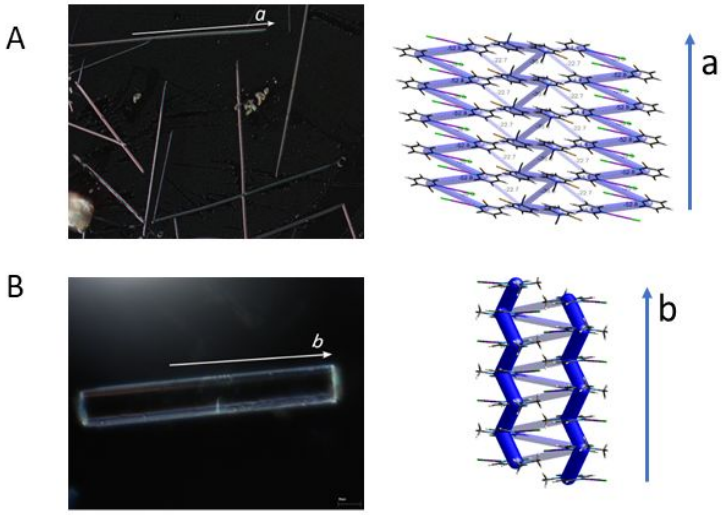

Figure 3. Microphotographs of the crystals PyBr·ICl (A) and Py(NMe_2)·ICl (B) and respective fragments of their energy frameworks.

Figures 2 and 3 (and Figure S6 in the Supporting Information) show that the evaluation of the energy framework topologies provides an adequate idea about the platelite of acicular habits of the HaB crystals of interhalogens. Furthermore, the diagonals of the rombic "blocks" in the energy frameworks of DABCO·IBr co-crystals match [001] and [010] directions indexed in their XRD experiment (Figure 4).

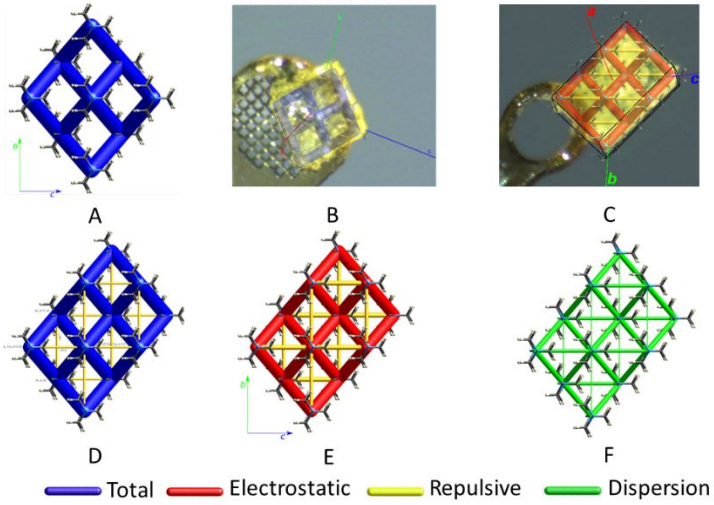

Figure 4. A) The total energy framework of DABCO·IBr; B) its overlay with the DABCO·IBr crystal; C) an overlay of DABCO·IBr crystal with the electrostatic component of energy framework; D) the attractive and repulsive components of the total interaction energy; E) electrostatic component (at 15 kJ/mol cut-off, see the framework at 20 kJ/mol cut-off in Figure S7 in the SI); and F) the dispersive component.

The energy decomposition analysis within the same framework (Figure 4D-F and Tables S1 and S2 in the Supporting Information) demonstrated that the [100] layers in the co-crystals of DABCO with ICl or IBr resulted from the predominantly electrostatic interactions between the DABCO·IX complexes. The repulsive interactions between the pairs of (x, y, z / x, y+1, z) and (3/2-x, 1-y, z-1/2 / 3/2-x, 1-y, z+1/2) molecules at the opposite corners of the rhomb are different (i.e. +15.3 kJ/mol *vs* +22.3 kJ/mol, respectively, Table S2 in the Supporting Information). Therefore, the crystal growth in the [010] direction (where repulsion between (x, y, z / x, y+1, z) pairs is weaker) may have some advantage over the growth in the [001] direction. A closer examination of DABCO·IBr revealed that indeed, some of crystals are elongated in [010] direction (Figure 2). The same consideration is applicable to co-crystals of DABCO with ICl (Table

S1 and Figure S8 the Supporting Information). This confirms that a detailed analysis of the energy framework of DABCO·IBr can explain small details of its crystal habit.

2.3. Computational analysis of the complexes of IX with DABCO and aromatic amines.

The short I…N separations in the co-crystals of IX with DABCO and pyridines (which were closer to a covalent bond than to van der Waals separations, vide supra) bring about the question of the nature of the interaction between these atoms. To elucidate this bonding, we examined electronic structures and topologies of the electron and energy densities of the complexes under study. Since their structural features in the solid-state can be distorted by the crystal forces, we compared their properties with those of the optimized complexes obtained via the M062X/def2tzvpp computations.[58] (Previous theoretical analyses indicated that this method produced excellent geometries and energies of HaB complexes at a reasonable computational cost, and therefore it was commonly used for analyzing the HaB systems, including very strong complexes similar to those in the current work.[40, 41, 59-65]). The characteristics of the HaB complexes resulting from these calculations are listed in Table 2.

Table 2. Interaction energies and interatomic distances in the HaB complexes[a]

Complex	ΔE, kJ/mol	$d_{I\cdots N}$, Å	$d_{I\cdots X}$, Å	Δq, e
DABCO·I_2	-62.1	2.387	2.824	0.27
DABCO·IBr	-83.6	2.334	2.662	0.28
DABCO·ICl	-91.3	2.322	2.509	0.28
$PyMe_2N$·ICl	-82.8	2.264	2.525	0.27
Py·ICl	-67.0	2.327	2.480	0.22
PyBr·ICl	-47.8	2.450	2.428	0.16
Phnz·IBr	-37.1	2.538	2.569	0.16

a) From the M062X/def2tzvpp calculations, see the Experimental section for details.

The interaction energies, ΔE, in the optimized complexes were consistent with the values evaluated using X-ray structural data (see Table 1) and with the high formation constants of 6.8×10^4 M^{-1} reported earlier for the 1:1 DABCO·I_2 complex.[35] Overall, they were intermediate between the typical HaB strength of about 4-20 kJ/mol and a covalent I-N bond of about 160 kJ/mol.[19, 66, 67] The I…N

separations in the calculated complexes were mostly within 0.05 Å of the value in the corresponding solid-state associations (Table 1). Also, the bond lengths and energies in the calculated complexes showed dependencies on the nature of XB donor and acceptors similar to that in the solid-state associations.

Very short interatomic N···I distances in all these (solid-state and optimized) complexes imply substantial orbitals' overlap (and interaction) of the interacting species. As a result, their molecular orbitals are delocalized over both the nucleophile and IX moieties (Figures S9 and S10 in the Supporting Information). The molecular-orbital delocalization was accompanied by a considerable polarization of the IX moiety and a substantial charge transfer from the nucleophile to the dihalogen. The analysis of charge distribution in these associations using quantum theory of atoms in molecules (QTAIM)[68] showed that the charges of the halogen-bonded iodine atoms vary from about +0.16e to +0.38e (Table S3 in the Supporting Information). The charges of the external X atoms vary from -0.43e to -0.65e. Accordingly, a charge transfer from the nucleophiles to IX molecules, Δq, was in a range from 0.16e to 0.28e (Table 2). Such a substantial charge transfer led to considerable elongations of I-X bond (Table 2) as compared to those in the individual IX molecules.

The QTAIM analysis [68,69] of the electron and energy densities, $\rho(\mathbf{r})$ and $H(\mathbf{r})$, at the bond critical points (BCPs) provided a valuable insight into the nature of the N···I and I···X bonds (Table 3). The highest electron densities were found at the BCPs on the N···I bond path in the solid-state associations with the shortest N···I bond lengths, i.e., DABCO·ICl and $PyNMe_2$·ICl. These values are close to 0.1 a.u. characteristic for the covalent bonds.[69] Similar electron density was found recently at the BCP of I···N bond between saccharin and hexamethylenetetramine, which pointed out its covalent character.[53] While the values of $\rho(r)$ in the complexes with the longer N···I bonds were somewhat lower, all of them were substantially larger than the values of about 0.01 a.u. typical for non-covalent halogen or hydrogen bonds [69-71]. Also, $\rho(r)$ values at BCPs of the N···I were comparable (somewhat higher or lower) to that at the adjacent I···X bonds in the same complex. Since electron densities at BCPs are highly correlated with the

strength of the bonds,[61, 69-72] these data suggest comparable strengths of the N···I and (originally intramolecular) I···X bonds.

Table 3. Electron and energy densities at BCPs in the HaB complexes[a]

Complex		$10^2\rho(r)$, a.u.		$10^2H(\mathbf{r})$, a.u.		BO(M)	
		N···I[b]	I···X[c]	N···I[b]	I···X[c]	N···I[b]	I···X[c]
DABCO·I_2	Opt	6.74	5.83	-1.85	-1.47	0.451	0.756
	Exp	6.82	5.64	-1.91	-1.36	0.486	0.735
DABCO·IBr	Opt	7.38	6.30	-2.27	-1.67	0.536	0.718
	Exp	7.87	5.86	-2.60	-1.43	0.587	0.676
DABCO·ICl	Opt	7.51	7.08	-2.37	-2.17	0.548	0.698
	Exp	8.26	5.94	-2.88	-1.48	0.628	0.624
$PyNMe_2$·ICl	Opt	8.00	6.81	-2.63	-2.01	0.522	0.673
	Exp	8.29	6.36	-2.83	-1.73	0.555	0.641
Py·ICl	Opt	7.06	7.46	-2.03	-2.43	0.449	0.741
	Exp	7.69	6.88	-2.43	-2.05	0.505	0.699
PyBr·ICl	Opt	5.45	8.26	-1.12	-2.99	0.325	0.829
	Exp	6.59	7.53	-1.73	-2.48	0.408	0.772
Phnz·IBr	Opt	4.67	7.50	-0.76	-2.42	0.281	0.872
	Exp	4.64	7.41	-0.75	-2.36	0.282	0.871

a) In the optimized (Opt) and solid-state experimental (Exp) complexes. b) At BCPs on the N···I bond path. c) At BCPs on the I···X bond path.

The total energy density at BCPs, $H(\mathbf{r})$, represents another feature which allows the identification of the nature of bonding. In particular, the negative values of $H(\mathbf{r})$ were associated earlier with the (partially) covalent characters of the corresponding bonds.[70,71] Indeed, all complexes under study are characterized by the negative $H(\mathbf{r})$ values at BCP along N…I bonds, and their magnitudes are comparable to those along the corresponding I…X bonds. As such the energy densities at BCPs also pointed out comparable strength and covalency of the N···I and I···X bonds.

These conclusions are supported by the Mayer Bond Order (MBO) indices, which quantify the degrees of bonding based on partitions of the electron density.[72,73] These indices generate the values which are consistent with the generally accepted bond orders in the simple covalent bonds. They provide valuable information about bonding in a variety of systems.[73] The experimental (solid-state) DABCO·ICl associations are characterized by the close MBO values of 0.63 and 0.62 for the N…I and I···X bonding,

respectively. These values are practically the same as the MBO for I-I bonds of 0.63 calculated in I_3^-. This indicates the analogy between bonding in the complexes under study and bonding in triiodide. The MBOs for I…N bonds in the DABCO·ICl, DABCO·IBr and $PyNMe_2$·ICl associations are also close to these values, and they decrease with the increase in the I…N separations.

The similarity (and covalent character) of the N···I and I···X interactions and their analogy to the bonding in I_3^- were corroborated by the Density Overlap Regions Indicator (DORI).[74] This method was recently developed for simultaneous visualization of both covalent and noncovalent interactions. DORI reveals the density overlap regions (bonds, intermolecular interactions, and steric clashes) showing deviations from the exponential dependences, and it identifies interactions using the sign of the 2nd eigenvalue of the density Hessian.[74] The DORI representations of the N…I and I…X bonding (Figure 5) were nearly identical and they were similar to those in the I_3^- anion. In all cases, these representations showed blue cylindrical isosurfaces, which are consistent with the covalent characteristics of these bonds. All these data indicated that the N…I…X interactions in the DABCO·IX complexes apparently represent an example of unsymmetrical four-electron three-center bonding.

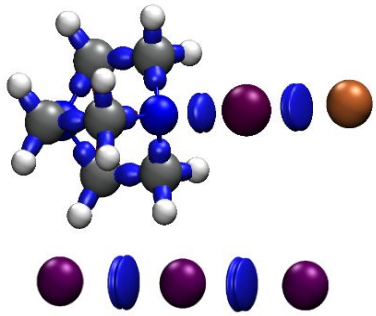

Figure 5. Visualization of bonding in DABCO·IBr (top) and I_3^- (bottom) via DORI isosurfaces (isodensity =0.95, $\nabla^2\rho(r)$) ranging from −0.4 au (blue) to 0.2 au (red).

3. Conclusions.

X-ray structural and computational analysis of the series of complexes of dihalogens IX (X=Cl, Br, I) with DABCO and pyridines revealed the relationship between the internal structural details and the crystal habits, and provided insights into the nature of the very strong halogen bonding. Although there are certain rules of thumb and concepts correlating the molecular crystals shapes with their supramolecular

structure, the results presented herein indicated direct relationship of the crystal habit with the pattern of the energy frameworks and the interplay of the attractive and repulsive interactions. Rationalization of the deformation of the rhombic crystal shape of DABCO with ICl and IBr based on a detailed analysis of their energy framework suggests the predictive potential of such an approach. On the other hand, the 1D chain-like topology of energy frameworks of pyridine and phanazine-based cocrystals clearly matches with their needle-like habit. As such, these results suggest a complementary approach to analyze the internal structure and the external shape of the crystals based on the energy framework scheme. It can be useful for visualizing the supramolecular architecture and rationalizing their mechanical behavior at the molecular level, for analyzing the long-range synthon aufbau modules (LSAMs) and supramolecular reactions,[75-77] as well as for rationalizing and predicting the crystal habit.

Our data also indicated that the variations in the HaB strength and length in the complexes under study were consistent with the changes in the maximum and/or minimum electrostatic potentials on the surface of the IX molecules and nucleophiles. Such correlations are common for the HaB supramolecular interactions. However, the very short I…N distances in these associations were much closer to the I···N covalent bond length than to the van der Waals separation. The characteristics of the N···I···X bonding in the complexes of IX with DABCO and pyridines were highly reminiscent of those in the I_2X^- anions (which was usually described as hypervalent 3c/4e bonding)[78,79] and in halonium cations.[62,63] In particular, they comprised positively-charged central iodine atoms and negatively-charged adjacent X and N atoms. The N···I distances in the complexes of IX with DABCO and pyridines are comparable to that in the iodonium complexes with the tertiary amines quinuclidine of 2.297 Å.[62] The experimental formation constant of the 1:1 DABCO·I_2 complex[35] is comparable to that of I_3^-,[80] and the I···X distances in these associations were within 0.1Å of those in the corresponding trihalides (see Table S4 in the Supporting Information). The QTAIM analysis of the topology of the electron and energy densities, MBO and DORY visualization confirmed the covalency of this bonding. All these results suggest that the interaction within

the IX complexes with DABCO and pyridines can be described as (unsymmetrical) hypervalent 3c/4e bonding similar to that in I_3^- and the halonium ions.

4. Experimental part

Materials. Commercially available DABCO, Phnz, I_2, ICl, and IBr were used without additional purification. Solvents were purified, dried, and distilled under an argon atmosphere before use.

Preparation of co-crystals. DABCO·ICl and DABCO·IBr. Addition of a solution containing 0.01 mmol of either IBr or ICl in 0.5ml of hexane to a solution of DABCO (0.01mmol) in hexane (0.5ml) instantly produced a yellow microcrystalline precipitate. The precipitate was filtered, washed with hexane, and dissolved in hot acetonitrile (1ml) in a water bath (~70°C). The clear yellow solution was allowed to cool down slowly to room temperature and was left overnight at 4°C. This resulted in well-formed yellow rhombic plates, which were suitable for single-crystal XRD.

Phnz·IBr. Addition of a solution containing 0.1mmol of IBr in 0.5 ml of hexane to a solution of phenazine (0.1mmol) in CH_2Cl_2 (0.2ml) produced a clear yellow solution, which was allowed to evaporate slowly at room temperature. In 72 h this resulted in well-formed long yellow needles, which were suitable for single-crystal XRD analysis.

Single crystals of ICl with Py, $PyNMe_2$, and PyBr were obtained in a similar way by slow evaporation of equimolar solutions of the respective pyridine and ICl in dichloromethane.

X-ray crystallographic analysis. The cell determination and the intensity data collection were performed using Bruker D8 Venture (DABCO·ICl, DABCO·IBr, and phnz·IBr) and Rigaku XtaLAB Synergy ($PyNMe_2$·ICl, Py·ICl, and PyBr·ICl) diffractometers equipped with graphite-monochromated Mo Kα radiation (0.71070 Å). The data for DABCO·ICl, DABCO·IBr, and phnz·IBr were collected by the standard ’phi-omega scan techniques, and were reduced using SAINT v8.37A.[81] SADABS software was used for scaling and absorption correction. Data collection, reduction and analysis for $PyNMe_2$·ICl, Py·ICl, and PyBr·ICl were performed with the CrysAlisPro software package (version 1.171.39.22a, Rigaku OD, 2018). All structures were solved by direct methods and refined by full-matrix least squares against F^2 using

Olex2 and SHELXTL software.[82,83] Non-hydrogen atoms were refined with anisotropic thermal parameters. All hydrogen atoms were geometrically fixed and refined using a riding model. Data for the new structures DABCO·ICl, DABCO·IBr, and phnz·IBr were deposited to CSD (see the details below); data for $PyNMe_2$·ICl, Py·ICl, and PyBr·ICl were used for their face indexing and identification (as matching with those deposited at CSD with codes: PYRIIC11, ZUDSEZ and GANXOJ respectively).

DABCO·ICl: Chemical formula $C_6H_{12}ClIN_2$, M = 274.53. Orthorhombic, *Pnma*, a = 21.6511 (17) Å, b = 6.9602 (6) Å, c = 5.9635 (5) Å, V = 898.68 (13) Å^3, Z = 4, T = 100 K, μ(MoKα) = 3.79 mm^{-1}, 12151 reflections measured, 1154 unique (R_{int} = 0.054). The final R1 was 0.026 (I > 2σ(I)) and wR2 was 0.065 (all data).

DABCO·IBr: Chemical formula $C_6H_{12}BrIN_2$, M = 318.99. Orthorhombic, *Pnma*, a = 21.6028 (9), Å, b = 7.1603 (3) Å, c = 5.9684 (2) Å, V = 923.21 (6) Å^3, Z = 4, T = 100 K, μ(MoKα) = 7.73 mm^{-1}, 8758 reflections measured, 1232 unique (R_{int} = 0.028). The final R1 was 0.016 (I > 2σ(I)) and wR2 was 0.036 (all data).

Phnz·IBr: Chemical formula $C_{12}H_8BrIN_2$, M = 387.01. Monoclinic, *C*2/*c*, a = 29.742(3), Å, b = 4.0442(4) Å, c = 21.075(2) Å, β=114.857(3)° , V = 2300.2(4) Å^3, Z = 8, T = 100 K, μ(MoKα) = 6.23 mm^{-1}, 14164 reflections measured, 3066 unique (R_{int} = 0.099). The final R1 was 0.040 (I > 2σ(I)) and wR2 was 0.086 (all data).

Complete crystallographic data, in CIF format, have been deposited with the Cambridge Crystallographic Data Centre. CCDC 2183013, 2183014 and 2236196 contains the supplementary crystallographic data for this paper. These data can be obtained free of charge via www.ccdc.cam.ac.uk/data_request/cif.

Computational details. Intermolecular interaction energy calculation and energy framework generation were performed using Crystal Explorer 17.5 (TONTO, B3LYP-DGDZVP) [52, 84, 85] for all unique molecular pairs in the first coordination sphere of a molecule (4.8Å), using experimental crystal geometries.

The individual amine·IX complexes were optimized with the Gaussian 09 suite of programs [86] using DFT (M062X [87]) calculations with the def2tzvpp [88] basis set. The coordinates extracted from the X-

ray structures of these associations were used as the starting points in the optimizations. The absence of the imaginary vibrational frequencies confirmed that the optimized structures represented true minima. Calculations in dichloromethane were carried out using a Polarizable Continuum Model.[89] This moderately polar solvent serves as a good media for modelling solid-state ionic compounds. The energies of interaction for all dyads were determined as: $\Delta E = E_{comp} - (E_{amine} + E_{IX}) + BSSE$, where E_{comp}, E_{amine}, and E_{IX} are sums of the electronic energies and ZPE of the complex and individual (optimized) amine and IX, and BSSE is a basis set superposition error.[90] The energies and coordinates of all experimental and optimized structures are listed in the Supporting Information.

The surface electrostatic potentials in Figure S2 in the Supporting Information were produced by single-point M062X/def2tzvpp calculation of individual optimized molecules. The V_{max} and V_{min} numbers (in kJ/mol) represent interaction energies of a positive test unity charge with the electric charge cloud generated by the molecules electrons and nuclei at each point of the molecular surface corresponding to the electron density isovalue of 0.001 e $bohr^{-3}$. [18,19]

The QTAIM analyses were carried out with the Multiwfn program.[91] The results were visualized using the molecular graphics program VMD.[92] The wfn output files for such an analysis were produced with Gaussian 09 via single-point M062X/def2tzvpp calculations using coordinates extracted from the experimental X-ray structures or optimized complexes. Since electron density calculations using M062X functional may produce substantial errors,[93] the results of such calculations were verified using MP2 method. The value of electron and densities produced by the MP2 calculations of selected complexes at BCPs along N…I and I….X bond paths were very close to that produced by the DFT M062X/def2tzvpp calculations (e.g. electron densities were 1-2% higher, and magnitudes of the negative energy densities were 3-4 % higher), and they verified conclusions made in this work.

Supporting Information. Fragments of the packing of DABCO·ICl, DABCO·IBr, and phnz·IBr, surface electrostatic potentials, details of the interaction energies decomposition in DABCO·ICl and DABCO·IBr, BFDH morphology simulation of DABCO·IBr, electrostatic component of energy frameworks of DABCO·ICl**,** molecular orbitals in the DABCO·I_2 complex, the I-X bond length in I_2X^-

anions, energies and atomic coordinates of the complexes The Supporting Information is available free of charge on the ACS Publications website at DOI: _____ .

Author contributions. Y. V. T. and S.V.R: conceptualization, investigation, data curation, visualization, writing – original draft, review and editing, D. H. and G.L: investigation, writing – review and editing.

Acknowledgments.

Y.T. thanks Kurnakov Institute of General and Inorganic Chemistry RAS for using the XRD equipment of shared experimental facilities. D.H. and S.V.R. thank the National Science Foundation (grant CHE-2003603) for financial support of this work. Calculations were done on Ball State University's beowulf cluster, which is supported by The National Science Foundation (MRI-1726017) and Ball State University.

References and notes.

1. Civati, F.; O'Malley, C.; Erxleben, A.; McArdle, P. Factors controlling persistent needle crystal growth: the importance of dominant one-dimensional secondary bonding, stacked structures, and van der Waals contact. *Cryst. Growth Des.* **2021**, *21*, 3449–3460.
2. Ito, S.; Nagai, S.; Ubukata, T.; Ueno, T.; Uekusa, H. Relationship between crystal structure, crystal morphology, and mechanochromic luminescence of triphenylimidazolylbenzothiadiazole derivatives. *Cryst. Growth Des.* **2020**, *20*, 4443–4453.
3. Li, C.; Shtukenberg, A. G.; Vogt-Maranto, L.; Efrati, E.; Raiteri, P.; Gale, J. D.; Rohl, A. L.; Kahr, B. Why are some crystals straight? *J. Phys. Chem. C* **2020**, *124*, 15616–15624.
4. Zhao, Y.; Tilbury, C. J.; Landis, S.; Sun, Y.; Li, J.; Zhu, P.; Doherty, M. F., A New software framework for implementing crystal growth models to materials of any crystallographic complexity. *Cryst. Growth. Des.* **2020,** *20*, 2885-2892
5. Shepelenko, M.; Hirsch, A.; Varsano, N.; Beghi, F.; Addadi, L.; Kronik, L.; Leiserowitz, L., Polymorphism, structure, and nucleation of cholesterol·H_2O at aqueous interfaces and in pathological media: revisited from a computational perspective. *J Am Chem Soc* **2022,** *144*, 5304-5314.
6. Aquilano, D.; Bruno, M.; Pastero, L., Impurity effects on habit change and polymorphic transitions in the system: aragonite–calcite–vaterite. *Cryst. Growth. Des.* **2020,** *20*, 2497-2507.

7. Zhang, S.; Zhou, L.; Yang, W.; Xie, C.; Wang, Z.; Hou, B.; Hao, H.; Zhou, L.; Bao, Y.; Yin, Q., An investigation into the morphology evolution of ethyl vanillin with the presence of a polymer additive. *Cryst. Growth. Des.* **2020,** *20*, 1609-1617.
8. Rosbottom, I.; Ma, C. Y.; Turner, T. D.; O'Connell, R. A.; Loughrey, J.; Sadiq, G.; Davey, R. J.; Roberts, K. J., Influence of solvent composition on the crystal morphology and structure of p-aminobenzoic acid crystallized from mixed ethanol and nitromethane solutions. *Cryst. Growth. Des.* **2017,** *17*, 4151-4161.
9. Hartman, P.; Bennema, P., The attachment energy as a habit controlling factor. *J. Crystal Growth* **1980,** *49*, 145-156.
10. Hartman, P.; Perdok, W. G., On the relations between structure and morphology of crystals. I. *Acta Crystall.* **1955,** *8*, 49-52.
11. Massaro, F. R.; Moret, M.; Bruno, M.; Rubbo, M.; Aquilano, D., Equilibrium and growth morphology of oligoacenes: periodic bond chains (PBC) analysis of tetracene crystal. *Cryst. Growth. Des.* **2011,** *11*, 4639-4646
12. Massaro, F. R.; Moret, M.; Bruno, M.; Aquilano, D., Equilibrium and Growth Morphology of Oligothiophenes: Periodic Bond Chain Analysis of Quaterthiophene and Sexithiophene Crystals. *Crystal Growth & Design* **2013,** *13* (3), 1334-1341.
13. Boerrigter, S. X. M.; Hollander, F. F. A.; van de Streek, J.; Bennema, P.; Meekes, H., Explanation for the needle morphology of crystals applied to a β' triacylglycerol. *Cryst. Growth. Des.* **2002,** *2*, 51-54.
14. *Mercury. Version 4.0. User Guide and Tutorials.* Cambridge Crystallographic Data Centre 2022.1 CSD Release.
15. Bravais, A. *Etudes Cristallographiques* (Paris: Gauthier Villars) 1866
16. Friedel, G., Études sur la loi de Bravais *Bull. Soc. Franc. Mineral*., **1907.** *30,* 326-455,
17. Donnay, J. D. H.; Harker D., A new law of crystal morphology extending the Law of Bravais *Am. Mineral.,* **1937,** 22, 446-467.
18. Bauzá, A.; Mooibroek, T. J.; Frontera, A. The bright future of unconventional σ/π-hole interactions. *ChemPhysChem* **2015**, *16*, 2496–2517.

19. Cavallo, G.; Metrangolo, P.; Milani, R.; Pilati, T.; Priimagi, A.; Resnati, G.; Terraneo, G. The halogen bond. *Chem. Rev.* **2016**, *116*, 2478–2601.

20. Mir, N. A.; Dubey, R.; Desiraju, G. R., Strategy and methodology in the synthesis of multicomponent molecular solids: the quest for higher cocrystals. *Acc. Chem. Res.* **2019,** *52*, 2210-2220.

21. Nangia, A. K.; Desiraju, G. R., Crystal engineering: an outlook for the future. *Angew Chem Int Ed* **2019,** *58*, 4100-4107.

22. Gunawardana, C. A.; Aakeroy, C. B., Co-crystal synthesis: fact, fancy, and great expectations. *Chem Commun* **2018,** *54*, 14047-14060.

23. Blagden, N.; Coles, S. J.; Berry, D. J. Pharmaceutical co-crystals - are we there yet? *CrystEngComm,* **2014,** 16, 5753-5761.

24. Zaworotko, M. J. Molecules to crystals, crystals to molecules ... and back again? *Cryst. Growth Des*, **2007**, *7*, 4-9.

25. Mir, N. A.; Dubey, R.; Desiraju, G. R., Four- and five-component molecular solids: crystal engineering strategies based on structural inequivalence. *IUCrJ* **2016,** *3* (Pt 2), 96-101.

26. Jones, D. K.; Gavvalapalli, N., Controlling the π-stack growth direction in organic π-conjugated microcrystals. *Cryst. Growth Des* **2021,** *22*, 1-19.

27. Okayasu, M.; Kikkawa, S.; Hikawa, H.; Azumaya, I., Relationship between crystal shape and unit cell shape: crystal shape modification via co-crystallization toward SXRD-suitable crystals. *CrystEngComm* **2021,** *23*, 7760-7770.

28. Torubaev, Y. V.; Skabitsky, I. V.; Anisimov, A. A.; Ananyev, I. V., Long-range supramolecular synthon polymorphism: a case study of two new polymorphic cocrystals of Ph2Te2–1,4-C6F4I2. *CrystEngComm* **2022,** *24*, 1442-1452.

29. Torubaev, Y.; Skabitsky, I.; Lyssenko, K. A., Stages of Kitaigorodsky Aufbau Principle detached in the cocrystals of Cp_2MX_2 (M = Ti, Zr; X = Cl, Br, I) with σ- and π-Hole Donors. *Cryst. Growth Des,* **2022**, *22,* 1244-1252**.**

30. Hassel, O. Structural aspects of interatomic charge-transfer bonding. *(* Nobel Lecture). *Science,* **1970,** *170,* 497-502. .

31. Pennington, W.T.; Hanks, T.W.; Arman, H.D. Halogen bonding with dihalogens and interhalogens *Struct. Bond.* **2008***, 126,* 65-104.

32. Walsh, R. B.; Padgett, C. W.; Metrangolo, P.; Resnati, G.; Hanks, T. W.; Pennington, W. T. Crystal engineering through halogen bonding: complexes of nitrogen heterocycles with organic iodides. *Cryst. Growth Des.* **2001**, *1*, 165-175.

33. Wu, W. X.; Liu, H. C.; Jin, W. J. Halogen bonding adsorbent pyridine n-oxides for iodine capture in water. *Chem. Eur. J.*, **2022**, *28*, e202103336.

34. Sutar, R. L.; Huber, S. M., Catalysis of organic reactions through halogen bonding. *ACS Catalysis* **2019,** *9*, 9622-9639.

35. Halpern, A.M.; Weiss, K.; Intramolecular pertrubation effects in diamine-iodine charge-transfer complexes. *J. Am. Chem. Soc.* **1968,** *90,* 6297 – 6302.

36. Santos, P. S.; Mello, M. T. S. The Raman spectra of some molecular complexes of 1-azabicyclo[2.2.2]octane and 1,4-diazabicyclo[2.2.2]octane. *J. Mol. Struct*. **1988**, *178*, 121-133.

37. Peuronen, A.; Valkonen, A.; Kortelainen, M.; Rissanen, K.; Lahtinen, M., Halogen bonding-based "catch and release": reversible solid-state entrapment of elemental iodine with monoalkylated DABCO salts. *Cryst. Growth Des.* **2012,** *12*, 4157-4169.

38. Aghabali, A.; Jun, S.; Olmstead, M.M.; Balch,A.L. Piperazine-functionalized C_{60} and diiodine or iodine monochloride as components in forming supramolecular assemblies *Dalton Trans.*, 2017, 46, 3710-3715.

39. Rheingold, A.L.; Baran, P.S. CCDC 2101978 CSD Communication(Private Communication)

40. Weinberger, C.; Hines, R.; Zeller, M.; Rosokha, S. V., Continuum of covalent to intermolecular bonding in the halogen-bonded complexes of 1,4-diazabicyclo[2.2.2]octane with bromine-containing electrophiles. *Chem Commun* **2018,** *54*, 8060-8063.

41. Borley, W.; Watson, B.; Nizhnik, Y.; Zeller, M.; Rosokha, S.V.; Complexes of diiodine with heteroaromatic N-oxides: effects of halogen-bond acceptors in halogen bonding. *J. Phys. Chem. A,* **2019***, 123*, 7113-7123.

42. Montis, R.; Arca, M.; Aragoni, M. C.; Blake, A. J.; Castellano, C.; Demartin, F.; Isaia, F.; Lippolis, V.; Pintus, A.; Lenardão, E. J.; Perin, G.; O'Connor, A. E.; Thurow S. Structural diversity in the products formed by the reactions of 2-arylselanyl pyridine derivatives and dihalogens," *New J. Chem.*, **2018**, 13, 10592–10602.

43. Batsanov, A.; Howard, J.; Lightfoot, A.; Twiddle, S.; Whiting, A. stereoselective chloro-deboronation reactions induced by substituted pyridine–iodine chloride complexes. *Eur. J. Org. Chem.* **2005**, *2005*, 1876–1883.

44. Jones, R. H.; Knight, K. S.; Marshall, W. G.; Clews, J.; Darton, R. J.; Pyatt, D.; Coles, S. J.; Horton, P. N., Colossal thermal expansion and negative thermal expansion in simple halogen bonded complexes. *CrystEngComm* **2014,** *16* (2), 237-243.

45. Awwadi, F. F.; Taher, D.; Kailani, M. H.; Alwahsh, M. I.; Odeh, F.; Rüffer, T.; Schaarschmidt, D.; Lang, H., Halogen bonding interactions in halopyridine–iodine monochloride complexes. *Cryst. Growth Des.* **2019,** *20* (2), 543-551.

46. Desiraju, G. R.; Parthasarathy, R. The Nature of halogen···halogen interactions: are short halogen contacts due to specific attractive forces or due to close packing of nonspherical atoms? *J. Am. Chem. Soc.* **1989**, 111, 8725– 8726.

47. Bondi, A. van der Waals volumes and radii *J. Phys. Chem.* **1964**, *68,* 441-451.

48. Chernyshov, I.Y.; Ananyev, I.V.; Pidko, E.A. Revisiting van der Waals radii: from comprehensive structural analysis to knowledge-based classification of interatomic contacts, *Chemphyschem* **2020,** *21,* 370-376.

49. Hennecke, U.;Muller, C.H.;Daniliuc, C.G. An enantioselective iodolactonization/cross-coupling protocol for the synthesis of highly substituted enol lactones *Eur.J.Org.Chem.*, **2018**, *2018,* 3158-3166.

50. Grebe, J.;Weller, F.; Dehnicke, K.N -Iodo-triphenylphosphaneimine. Synthesis and crystal structures of [Me3SiNPPh3·ICl] and Ph_3PNI *Naturforsch.,B:Chem.Sci.* **1996**, *51,* 1739-1743.
51. Computational Chemistry Comparison and Benchmark Database Release 22, Standard Reference Database 101 National Institute of Standards and Technology (May 2022)
52. Mackenzie, C. F.; Spackman, P. R.; Jayatilaka, D.; Spackman, M. A. CrystalExplorer model energies and energy frameworks: extension to metal coordination compounds, organic salts, solvates and open-shell systems *IUCrJ*, **2017**, 5, 575–587.
53. Anyfanti,G.; Bauzá, A.; Gentiluomo, L; Rodrigues, J.; Portalone, G.; Frontera, A.; Rissanen, K.; Puttreddy, R. Short X···N halogen bonds with hexamethylenetetraamine as the acceptor. *Frontiers in Chem.* **2021**, *9*, 623595.
54. Lucassen, A. C. B.; Karton, A.; Leitus, G.; Shimon, L. J. W.; Martin, J. M. L.; van der Boom, M. E. Co-crystallization of sym-triiodo-trifluorobenzene with bipyridyl donors: consistent formation of two instead of anticipated three N···I halogen bonds. *Cryst. Growth Des.* **2007**, *7*, 386–392.
55. Frey, M.; Genovesio-Taverne, J.-C.; Fontecilla-Camps, J. C. Application of the periodic bond chain (PBC) theory to the analysis of the molecular packing in protein crystals. *J. Cryst. Growth* **1988,** *90*, 245-258.
56. Torubaev, Y. V.; Skabitsky, I. V.; Saratov, G. A.; Barzilovich, P. Y., Halogen vs. ionic bonding: an unusual isomorphism between the neutral (C5Me5)(2)Fe/C2I2 cocrystal and ionic (C5Me5)(2)Fe Br-3 crystal. *Mendeleev Communications* **2021,** *31*, 58-61.
57. Bairagi, K. M.; Ingle, K. S.; Bhowal, R.; Mohurle, S. A.; Hasija, A.; Alwassil, O. I.; Venugopala, K. N.; Chopra, D.; Nayak, S. K. Interplay of halogen and hydrogen bonding through co-crystallization in pharmacologically active dihydropyrimidines: insights from crystal structure and energy framework *ChemPlusChem*, 2021, *86*, 1167-1176.
58. Zhao, Y.; Truhlar, D. G. The M06 suite of density functionals for main group thermochemistry, thermochemical kinetics, noncovalent interactions, excited states, and transition elements: two new

functionals and systematic testing of four M06-class functionals and 12 other functionals. *Theor. Chem. Acc.* **2008**, *120*, 215.

59. Bauzá, A.; Alkorta, I.; Frontera,A.; Elguero, J. *Chem. Theory Comput.,* **2013**, *9*, 5201.
60. Zhu, Z.; Xu, Z.; Zhu,W. Interaction nature and computational methods for halogen bonding: a perspective. *J. Chem. Inf. Model*. **2020**, *60*, 2683.
61. Miller, D.K.; Loy, C.; Rosokha, S.V.; Examining a transition from supramolecular halogen bonding to covalent bonds: topological analysis of electron densities and energies in the complexes of bromosubstituted electrophiles. *ACS Omega*, **2021**, 6, 235888-23597
62. Ward, J.S.; Frontera, A.; Rissanen, K. Iodonium complexes of the tertiary amines quinuclidine and 1-ethylpiperidine *Dalton Trans.*, **2021**,50, 8297-8301
63. Ward, J.S.; Frontera, A.; Rissanen, K. Asymmetric $[N–I–N]^+$ halonium complex *Chem. Commun.*, **2020**,56, 8428-8431
64. Bauzá, A.; Alkorta, I.; Frontera,A.; Elguero, J. On the reliability of pure and hybrid dft methods for the evaluation of halogen, chalcogen, and pnicogen bonds involving anionic and neutral electron donors *Chem. Theory Comput.,* **2013**, *9*, 5201.
65. Rosokha, S. V.; Stern, C. L.; Ritzert, J. T. Experimental and computational probes of the nature of halogen bonding: complexes of bromine-containing molecules with bromide anion. *Chem. Eur. J.*, **2013**, *19*, 8774-8788.
66. Sarwar, M. G.; Dragisic, B; Salsberg, L. J.; Gouliaras, C.; Taylor, M. S. Thermodynamics of halogen bonding in solutions: substituents, structural and solvent effects. *J. Am. Chem. Soc.* **2010**, 13*2*, 1646-1653.
67. T. L. Cottrell, The strengths of chemical bonds, 2d ed., Butterworth, London, 1958.
68. Bader, R. F. W. A quantum theory of molecular structure and its applications. *Chem. Rev.***1991**, *91*, 893 - 928.
69. Matta C.F. , Boyd R.J. Eds. *The quantum theory of atoms in molecules, from solid state to DNA and drug design* Wiley VCH Weinheim 2007.

70. P. L. A. Popelier, The QTAIM perspective of chemical bonding in *The Chemical Bond*, John Wiley & Sons, Ltd, **2014**, p. 271.

71. Espinosa, E.; Alkorta, I.; Elguero, J.; Molins, E. From weak to strong interactions: a comprehensive analysis of the topological and energetic properties of the electron density distribution involving X–H···F–Y systems. *J. Chem. Phys.* **2002**, *117*, 5529.

72. Mayer, I. Bond order and valence indices: A personal account. *J. Comp. Chem.* **2007**, *28* , 204–221.

73. Bridgeman, A.J.; Cavigliasso, G.; Ireland,L.R.; Rothery J. The Mayer bond order as a tool in inorganic chemistry *J. Chem. Soc., Dalton Trans*., **2001**, 2095–2108.

74. de Silva, P.; Corminboeuf, C. Simultaneous visualization of covalent and noncovalent interactions using regions of density overlap. *J. Chem. Theory Comput.* **2014**, *10*, 3745–3756.

75. Torubaev, Y. V.; Skabitsky, I. V., A new supramolecular heterosynthon [C–I···OC(carboxylate)] at work: engineering copper acetate cocrystals. *CrystEngComm* **2020,** *22* (40), 6661-6673.

76. Torubaev, Y. V.; Skabitsky, I. V., The energy frameworks of aufbau synthon modules in 4-cyanopyridine co-crystals. *CrystEngComm* **2019,** *21* (46), 7057-7068.

77. Torubaev, Y. V.; Rai, D. K.; Skabitsky, I. V.; Pakhira, S.; Dmitrienko, A., Energy framework approach to the supramolecular reactions: interplay of the secondary bonding interaction in Ph_2E_2 (E = Se, Te)/ *p*-I-$C_6F_4I_2$ co-crystals. *New J. Chem.,* **2019,** *43* (21), 7941-7949.

78. Svensson, P.H.; Kloo, L. Synthesis, structure, and bonding in polyiodide and metal iodide-iodine systems *Chem. Rev.* **2003,** *103,* 1649 – 1684.

79. Li, D.; Xia, T.; Feng, W.; Cheng, L. Revisiting the covalent nature of halogen bonding: a polarized three-center four-electron bond. *RCS Advances,* **2021,** *11,* 32852-32860.

80. Encyclopedia of electrochemistry of the elements. V. 1.; Bard, A. J., Ed.; Marcel Dekker, Inc.: New York, 1973; pp 1−148.

81. *Bruker Apex3 v2016.9-0, SAINT V8.37A,* Bruker AXS Inc.: Madison, WI, 2016.

82. Dolomanov, O. V.; Bourhis, L. J.; Gildea, R. J.; Howard, J. A. K.; Puschmann, H., OLEX2: A complete structure solution, refinement and analysis program *J. Appl. Cryst.* **2009,** *42* (2), 339-341.

83. Sheldrick, G. M., Crystal structure refinement with SHELXL. *Acta Crystallographica Section C Structural Chemistry* **2015,** *71* (1), 3-8.

84. Spackman, P. R., Turner, M. J., McKinnon, J. J., Wolff, S. K., Grimwood, D. J., Jayatilaka, D.; Spackman, M. A. *CrystalExplorer*: a program for Hirshfeld surface analysis, visualization and quantitative analysis of molecular crystals. *J. Appl. Cryst.* **2021**,*54,* 1006–1011

85. Turner, M.J.; Thomas, S.P.; Shi, M.W.; Jayatilaca, D. Spackman, M.A. Energy frameworks: insights into interaction anisotropy and the mechanical properties of molecular crystal. *Chem. Commun.*, **2015**, *51*, 3735-3738

86. Frisch, M. J.; Trucks, G. W.; Schlegel, H. B.; Scuseria, G. E.; Robb, M. A.; Cheeseman, J. R.; Scalmani, G.; Barone, V.; Mennucci, B.; Petersson, G. A., et al. *Gaussian 09, Revision C.01,* Gaussian, Inc., Wallingford CT, 2009. Gaussian.

87. Zhao, Y.; Truhlar, D. G. The M06 Suite of Density Functionals for Main Group Thermochemistry, Thermochemical Kinetics, Noncovalent Interactions, Excited States, and Transition Elements: Two New Functionals and Systematic Testing of Four M06-Class Functionals and 12 Other Functionals. *Theor. Chem. Acc.* **2008**, *120*, 215–241.

88. Weigend, F.; Ahlrichs, R. Balanced basis sets of split valence, triple zeta valence and quadruple zeta valence quality for H to Rn: Design an assessment of accuracy. Phys. Chem. Chem. Phys. **2005,** *7*, 3297-3305.

89. Tomasi, J.; Mennucci, B.; Cammi, R. Quantum mechanical continuum solvation models. *Chem. Rev.***2005**, *105*, 2999.

90. Boys, S. F.; Bernardi, F. The calculation of small molecular interactions by the differences of separate total energies. some procedures with reduced errors. *Mol. Phys*. **1970**, *19*, 553−566.

91. Lu, T.; Chen, F. Multiwfn: a multifunctional wavefunction analyzer. *J. Comput. Chem.* **2012**, *33*, 580–592.

92. Humphrey, W.; Dalke, A.; Schulten, K. VMD – Visual Molecular Dynamics. *J. Mol. Graphics* **1996**, *14*, 33–38.

93. Mezei, P.D., Csonka, G.I.; Kállay, M. Electron density errors and density-driven exchange-correlation energy errors in approximate density functional calculation *J. Chem. Theory Comput*. **2017**, *13*, 4753–4764.